In-Flight Pressure Distribution Measurements; instrumentation, data handling and comparison with windtunnel data

H. Kannemans
National Aerospace Laboratory NLR
Anthony Fokkerweg 2, 1059 CM Amsterdam
the Netherlands
and
D.F. Volkers
Fokker Aircraft B.V.
P.O. BOX 7600, 1117 ZJ Schiphol
the Netherlands

Summary

As part of the certification of the Fokker 100 aircraft, in-flight wing pressure distributions were measured.

The objective of the analysis presented in the present paper is to make a comparison of flight test data with windtunnel data.
To this end an accurate calibration was made of the in-flight angle of attack, providing the appropriate reference conditions used for the comparison with windtunnel data.

Corrections were applied for differences in wing shape, due to differences in flight test and windtunnel conditions as well as due to production tolerances. This way the validity of the testmethods and available extrapolation techniques was investigated. The results of this investigation confirm that for the type of wing section used in the Fokker 100, full-scale characteristics of the wing can be predicted from windtunnel model experiments.

Nomenclature

a	speed of sound
b	span of main wing
c	local chord
c_1	local lift coefficient
c_{1_α}	lift curve slope
c_m	local pitch moment coefficient about $x_w=0.25c$
c_M	Mach number derivative
c_p	$(p-p_\infty)/q_\infty$
c_{qV}	pitch rate derivative
c_R	calibration correction for an offset in sideslip
c_{RB}	calibration correction for sideslip influence
$c_{Y\beta}$	sideslip derivative of the dimesionless sideforce
c_o	basic coefficient
c_α	angle of attack derivative
g	acceleration due to gravity
h	altitude
$\dot{h}$	dh/dt
m	mass of the aircraft
M	Mach number
n	normal load factor
p	presssure
$p_{s\infty}$	undisturbed static pressure
$\dot{p}_{s\infty}$	$dp_{s\infty}/dt$
q	pitch rate
q_∞	dynamic pressure
Re_c	Reynolds number based on mean aerodynamic chord
S	area of the main wing
t	time
u	velocity component along x_{body} axes
v	velocity component along y_{body} axes
V	true airspeed
V_E	see figure 5
V_N	see figure 5
V_X	see figure 5
V_Y	see figure 5
w	velocity component along z_{body} axes
WT	windtunnel
x	x_{body} axes along fuselage centreline, positive pointing forward
x_w	chordwise position ($x_w=0$ is the leading edge)
X	see figure 5
y	y_{body} axes perpendicular to x and z axes
Y	see figure 5
z	z_{body} axes in plane of symmetry perpendicular to x axes
α	angle of attack as determined from h
α_c	calibrated angle of attack (relative to fuselage centreline)
α_1	angle of attack readings of the left fuselage vane
α_2	angle of attack readings of the right fuselage vane
β	angle of sideslip
$\Delta\alpha$	α offset
$\Delta\beta$	β offset
$\Delta\beta_o$	bias due to sideslip
$\Delta\Theta$	wing deformation
ρ	density of air
η	y/b
Θ	pitch angle
ϕ	bank angle
Ψ	heading

1. Introduction

As part of the certification of the Fokker 100 aircraft, it was decided that in-flight pressure distribution measurements were required on the main wing. The measurements were performed by Fokker in order to verify the wing loading and to compare flight test data with windtunnel data for design process validation purposes. Pressure distributions were measured at a number of chordwise sections of the main wing, using pressure belts. These belts consist of plastic tubes which were attached to the wing surface of the test aircraft. The pressure tubes at these measurement sections were connected to several scanivalves. The measurement data delivered by the scanivalves as well as data defining the flight condition were recorded on tape. Data processing was performed by the National Aerospace Laboratory (NLR). The main goal of the data reduction was to compute the aerodynamic coefficients c_p as accurately as possible applying various corrections and interpolations.

In the past in-flight pressure distribution measurements were performed by many investigators (Refs. 1 through 7); usually correlation with windtunneldata was one of their main purposes. An interesting point, which has not been highlighted in literature in much detail up to now, is that verification of the results with windtunneldata is only possible if the relation between flight test condition and windtunnel condition is known at all cases of interest. Here the conditions cover the subsonic flight regime for level flight and the transonic flight region for a range of load factors. For the analysis presented here, the angle of attack vanes, located at the fuselage, was calibrated accurately in order to provide the true in-flight angle of attack to be used for comparison with windtunnel data. Also corrections are required for the difference in wing shape between model and aircraft due to deformation and production deviations.

2. Instrumentation

The in-flight wing pressure measurements were obtained from five rows of orifices on the upper and lower surfaces of the main wing (three on the right wing, two on the left wing) at the span stations shown in figure 1. The chordwise locations of the 30 flight wing pressure orifices in each row are presented in table 1. The chordwise extent of the pressure belt at the sections 1 and 2 was limited to 80 percent of the local chord on upper and lower surface because of the presence of the aileron. At the flap, present in the sections 3,4 and 5, it was possible to take pressure measurements as long as the flaps were retracted (take-off with retracted flaps; the pressure tubes were disconnected by a deflection of the flap). The pressure belts made of plastic multitubes were taped to the wing surface (see Fig. 2) with the pressure orifices located in each of the multiple tubes. The 150 pressure holes were connected to four scanivalves (the cycle period of the scanivalve is 4.8 sec, number of ports is 48), each provided with one Druck differential transducer. For each scanivalve the pressure difference of two holes was also measured continuously by an accurate Rosemount differential transducer (see Fig. 3). From this simultaneous pressure measurement a scale factor has been obtained for the less accurate Druck transducer
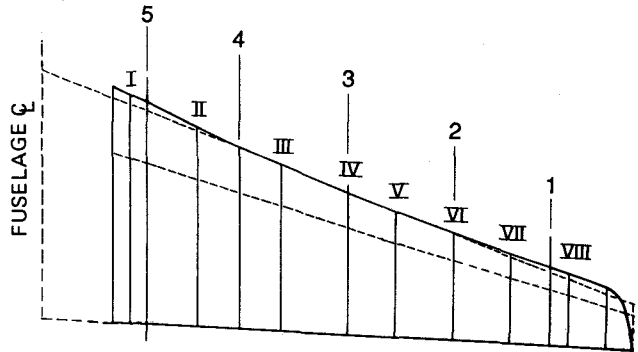

FIGURE 1 – Measurement sections on the Fokker 100 main wing.
(flight: test sections at right wing 2,3,4; test sections at left wing 1,5 windtunnelmodel: test sections I through VIII)

TABLE 1 Nominal positions of pressure orifices

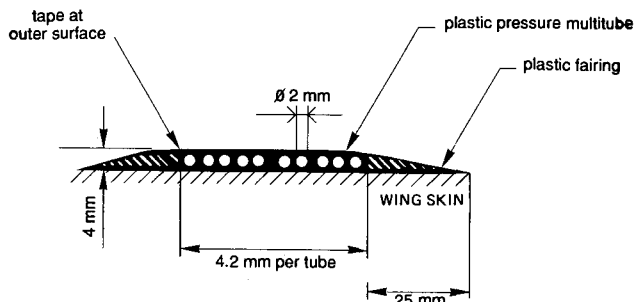| positions $100x_w/c$	measurement section number -->				
	1	2	3	4	5
upper surface					
98			x	x	x
90			x	x	x
80	x	x	x	x	x
70	x	x	x	x	x
60	x	x	x	x	x
55	x	x	x	x	x
50	x	x	x	x	x
45	x	x	x	x	x
40	x	x	x	x	x
35	x	x	x	x	x
30	x	x	x	x	x
25	x	x	x	x	x
20	x	x	x	x	x
15	x	x	x	x	x
10	x	x	x	x	x
5	x	x	x	x	x
2	x	x	x	x	x
1	x	x			
0	x	x	x	x	x
lower surface					
1	x	x			
2	x	x	x	x	x
5	x	x	x	x	x
10	x	x	x	x	x
20	x	x	x	x	x
25	x	x			
30	x	x	x	x	x
35	x	x			
40	x	x	x	x	x
50	x	x	x	x	x
60	x	x	x	x	x
70	x	x	x	x	x
80	x	x	x	x	x
90			x	x	x
98			x	x	x

1497

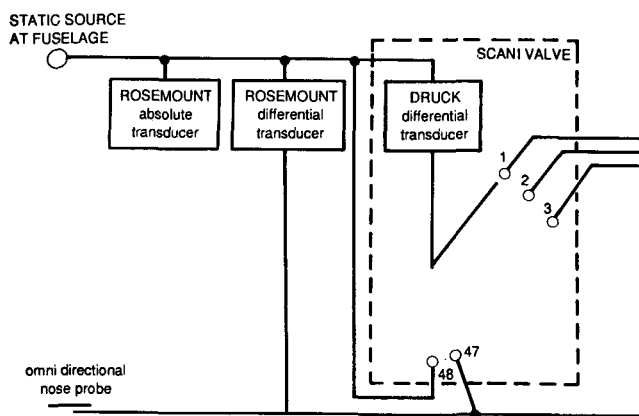FIGURE 2 - Cross section of the pressure belt

FIGURE 3 - Schematic diagram of pressure measuring system

during each cycle.
Besides the pressure distribution measurements, parameters defining the flight condition have to be measured as well. They are: impact pressure, static pressure, total air temperature, readings of the angle of attack vanes at the fuselage, readings of the angle of sideslip vane at the fuselage and the body accelerations and attitude of the aircraft using an inertial reference system.
The onboard data acquisition system performed the tasks of signal conditioning, sampling and storage on magnetic tape.

After calibration the accuracies of the measured parameters were as listed in Table 2.

3. Test programme

The pressure distribution measurements were taken in stabilized flight at various flight levels, speeds, normal load factors (by varying the bank angle) and flap settings. During flights the scanivalves were stepping continuously to produce about ten cycles of readings in each run. Only 21 runs (clean configuration, different conditions) from a much larger amount of measurement runs were used in the actual analysis.

These runs can be split up into two groups: (1) subsonic flight regime (at one flight level with load factor 1 and varying speeds); (2) transonic flight regime (at one flight level with varying load factors between 1 and 2 and varying Mach numbers; see table 3).

TABLE 3 Measurement runs used for the validation analysis

run number	flight level ft	velocity/ Mach number	approximate normal load factor n	nominal bank angle deg
33	24000	M=0.7	1.0	0
35	24000	M=0.7	1.5	-48
39	24000	M=0.7	2.0	-60
41	24000	M=0.72	1.0	0
47	24000	M=0.72	1.5	48
49	24000	M=0.72	2.0	60
51	24000	M=0.75	1.0	0
53	24000	M=0.75	1.5	-48
55	24000	M=0.75	2.0	-60
57	24000	M=0.78	1.0	0
59	24000	M=0.78	1.5	48
61	24000	M=0.78	2.0	60
81	10000	200kCAS	1.0	0
83	10000	190kCAS	1.0	0
85	10000	180kCAS	1.0	0
87	10000	170kCAS	1.0	0
89	10000	160kCAS	1.0	0
91	10000	150kCAS	1.0	0
93	10000	139kCAS	1.0	0
95	10000	128kCAS	1.0	0
97	10000	118kCAS	1.0	0

TABLE 2 Measurement variables

Parameter	Name	Unit	Range	Resol.	Accur.	Samp.fr.	Symbol	Remarks
angle of attack left	AAV1	deg	-20/60	0.01		16	α_1	
angle of attack right	AAV2	deg	-20/60	0.01		16	α_2	
angle of sideslip	ASV	deg	-40/40	0.02	0.02	16		
press. diff. scanivalve	PDSV.R	kPa	-35/35	0.017	0.05%	0.21		4X
scanivalve pressures	PWEX...	kPa	-35/35	0.02	0.25%	0.21		184X
scan. reference press.	PSRSCAN	kPa	10/110	0.0002	0.02%	16		1X
impact pressure	PI	kPa	0/35	0.00008	0.04%	16		
static pressure	PS	kPa	10/110	0.0002	0.02%	16		
total air temperature	TAT	CEL	-60/60	0.05	1%	8		
angle of pitch	APIRS	deg	-180/180	0.0055	0.05	50	θ	from IRS (Inertial Reference System)
bank angle	ARIRS	deg	-180/180	0.0055	0.05	50	ϕ	
Y acceleration	AYBIRS	m/s2	-39/39	0.0024	0.005	50	A_Y	

4. Data reduction

The flight test data were read from the flight test tape by the data reduction station DVSV, calibrated and transferred to the NLR Cyber 180-855 mainframe computer. Processing of the in-flight pressure data was performed by the program PRESS to compute the aerodynamic coefficients c_p.

This program makes use of the NPP (NLR Post Processing) database software package (see Fig. 4).
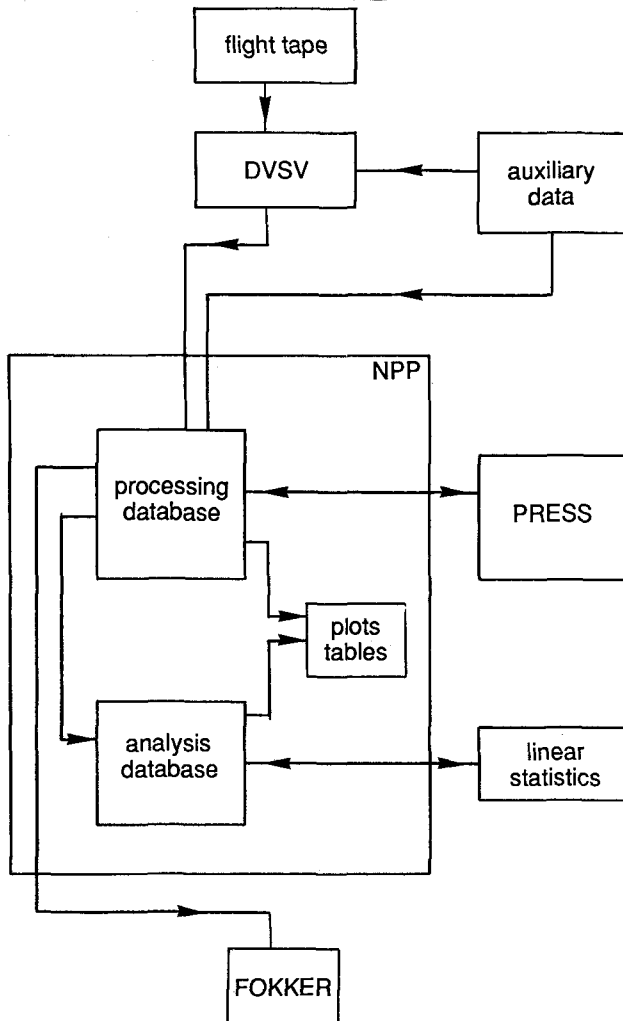

FIGURE 4 - Data processing scheme

Although much attention was paid to keep the flow condition constant during the flight tests, deviations from the initial condition of the recordings are unavoidable. This fact was accounted for during the dataprocessing. Pressure distributions in the form of 'snap shots' were computed for each scanivalve cycle.
The main functions of the data reduction program PRESS are to provide:
- linear time interpolations of the measured time series,
- corrections for time delays in all the pressure tubes (time delays are less than 1 sec),
- application of position error corrections to the reference static pressure hole and to the total pressure probe,
- computations of the momentaneous aerodynamic coefficients c_p,
- quick-look monitoring of momentaneous pressure distributions of each scanivalve cycle.

5. Calibration of the angle of attack vanes at the fuselage

Accurate calibration of the in-flight angle of attack (especially at the transonic flight regime and for normal load factors up to 2) is of major importance for the validation and interpretation of the pressure distribution measurement results. It was decided to use the calibrated angle of attack vane readings instead of flight path reconstruction (estimation) for validation purposes. The reason for this is that the airload is a function of the aerodynamic angle of attack while the flight path may deviate due to the wind field being of a rather complicated behaviour especially at conditions during flight turn manoeuvres (normal load factor larger than 1). The determination of the angle of attack calibration equation as described in the present paper requires the combination of runs with varying bank angle (left and right turning manoeuvres as well as level flight) and varying Mach numbers. The redundant information of these combined runs was used to estimate the calibration equation accurately by regression analysis. This calibration procedure will be described in three steps:
- computation of a theoretical angle of attack from the pressure altitude variation and the attitude of the aircraft during flight turning manoeuvres,
- estimation of the angle of attack calibration equation by means of regression analysis,
- application of the calibration equation to the measured data.

5.1 Computation of a theoretical angle of attack from the pressure altitude variation

This computation can be split up in four steps:
- computation of the pressure altitude variation,
- determination of the sideslip angle,
- extraction of the angle of attack from the pressure altitude variation,
- determination of the offset in the angle of attack due to sideslip uncertainties.

- Computation of the pressure altitude variation.
The pressure altitude variation can be computed from:

$$\dot{h} = - \frac{\dot{p}_{s\infty}}{g\rho} \qquad (1)$$

- Determination of the sideslip angle
The computation of the angle of attack from the pressure altitude variation during a turning manoeuvre requires the availability of sideslip data. The sideslip angle was computed (estimated) using the body acceleration A_y from:

$$\beta = \frac{mA_y}{\frac{1}{2}\rho V^2 S C_{y\beta}} \qquad (2)$$

1499

where $C_{y\beta}$ is the side force derivative coefficient with respect to the sideslip determined during earlier flight tests. Note that the measurement runs were flown close or equal to zero degrees slip angle.

- Extraction of the angle of attack from the pressure altitude variation.
The analysis starts from the well-known transformation equations:

$$u = V_N \cos\Theta\cos\Psi + V_E \cos\Theta\sin\Psi + \dot{h}\sin\Theta \qquad (3)$$

$$v = V_N(\sin\phi\sin\Theta\cos\Psi - \cos\phi\sin\Psi) + V_E(\sin\phi\sin\Theta\sin\Psi$$
$$+ \cos\phi\cos\Psi) - \dot{h}\sin\phi\cos\Theta \qquad (4)$$

$$w = V_N(\cos\phi\sin\Theta\cos\Psi + \sin\phi\sin\Psi) + V_E(\cos\phi\sin\Theta\sin\Psi$$

$$- \sin\phi\cos\Psi) - \dot{h}\cos\phi\cos\Theta \qquad (5)$$

where u, v, w are the velocity components along the body axes and V_N(north), V_E(east), $\dot{h}$(vertical) are the velocity components along an earth fixed coordinate system (fig. 5). Here the velocity vector (u,v,w) as well as the velocity vector $(V_N, V_E, -\dot{h})$ are defined as the momentaneous velocity of the aircraft relative to the surrounding air.
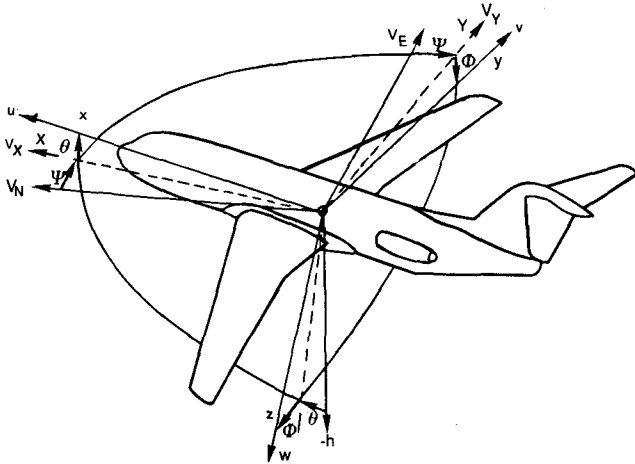
FIGURE 5 - Applied coordinate system and sign conventions

For further analysis the next transformation is essential (see fig. 5):

$$V_X = V_E \sin\Psi + V_N \cos\Psi \qquad (6)$$

$$V_Y = V_E \cos\Psi - V_N \sin\Psi \qquad (7)$$

where V_X is directed along the projection of the x_{body} axes onto the horizontal plane. Substitution of (6) and (7) into (3),(4) and (5) yields:

$$u = V_X \cos\Theta + \dot{h}\sin\Theta \qquad (8)$$

$$v = V_X \sin\phi\sin\Theta + V_Y \cos\phi - \dot{h}\sin\phi\cos\Theta \qquad (9)$$

$$w = V_X \cos\phi\sin\Theta - V_Y \sin\phi - \dot{h}\cos\phi\cos\Theta \qquad (10)$$

Substitution of $v = V\sin\beta$ into (9) results in:

$$V_Y = \frac{\dot{h}\sin\phi\cos\Theta - V_X\sin\phi\sin\Theta + V\sin\beta}{\cos\phi} \qquad (11)$$

From

$$V^2 = V_X^2 + V_Y^2 + \dot{h}^2 \qquad (12)$$

it follows that:

$$V_X = \sqrt{V^2 - V_Y^2 - \dot{h}^2} \qquad (13)$$

Equations (11) and (13) form a couple of nonlinear equations which can be solved iteratively starting from equation (11) with $V_{X(initial)}=V$. The angle of attack can be computed by substitution of $w=V\cos\beta\sin\alpha$ into (10):

$$\alpha = \sin^{-1}\frac{V_X\cos\phi\sin\Theta - V_Y\sin\phi - \dot{h}\cos\phi\cos\Theta}{V\cos\beta} \qquad (14)$$

- Influence of the sideslip uncertainties on the angle of attack.
A first order simplification of equation (11) yields:

$$\Delta V_Y = \frac{V\Delta\beta}{\cos\phi} \qquad (15)$$

and equation (14) can be simplified to:

$$\Delta\alpha = -\frac{\Delta V_Y \sin\phi}{V} \qquad (16)$$

Combining (15) and (16) results in:

$$\Delta\alpha = -\Delta\beta\, tg\phi \qquad (17)$$

Thanks to the fact that left and right turning manoeuvres are combined before regression the $\Delta\beta$ offset can be estimated very well as will be shown later ($\Delta\beta$ is estimated to be 0.1 deg).

5.2 Estimation of the angle of attack calibration equation by means of regression

Two steps are distinguished:
- to set up the regression equation,
- analysis of the regression equation by deleting non-significant terms.

- Set up of the regression equation
The following regression equation was used in the analysis:

$$\alpha = c_o + \tfrac{1}{2}c_\alpha(\alpha_1+\alpha_2) + c_M M + 14 c_{qV} q/V + c_R tg\phi$$
$$+ c_{RB}\beta tg\phi \qquad\qquad (18)$$

where the following constants have to be estimated:

$c_o = \alpha_o$ (offset)

$c_\alpha = d\alpha/d\alpha_{vane\ readings}$ (calibration factor)

$c_M = d\alpha/dM$ (Mach number effect)

$c_{qV} = d\alpha/d(14q/V)$ (pitch rate effect due to an armlength of 14m)

$c_R = d\Delta\alpha/dtg\phi = -\Delta\beta_o$ ($\Delta\beta$ offset)

$c_{RB} = d\Delta\alpha/d\beta tg\phi$ (additional calibration on $\Delta\beta$)

Note that the left hand side parameter α (eq. 18) is hardly influenced by the windvector (small random deviations only) because of the fact that (1) its value is computed from the pressure altitude variation and (2) the direction of flight (and as a consequence the direction of the wind relative to the aircraft)was varying over the manoeuvres to be combined.

- Analysis of the regression equation
Equation (18) has been analysed for two separate cases:
- calibration equation for subsonic conditions (M<0.4),

- calibration equation for transonic conditions (0.7≤M<0.8).

- Calibration equation for subsonic conditions
The regression analysis is based on nine combined runs (table 3) taken at subsonic speeds and level flight. At these conditions the influence of sideslip on the angle of attack calibration is supposed to be negligible and can be omitted in the regression equation (18).
From regression analysis (see table 4) it follows that the standard error of the estimated calibration factor c_α is σ_α=0.2%. In addition it became clear that the influence of the Mach number c_M and the influence of the pitch rate c_{qV} may not be neglected.
The resulting calibrated angle of attack α_c and the originally computed angle of attack α are both plotted in figure 6.

- Calibration equation for transonic conditions
The regression analysis is based on 12 combined runs (table 3) taken at transsonic speeds and one flight level with varying load factors between 1 and 2 and varying speeds: M=.7,.72,.75,.78.
A first analysis did show that the term c_{RB} is of a non-significant value and can be omitted. From a physical point of view this means that the adopted sideslip angle $\beta(A_Y)$ does not need further calibration to improve the accuracy of the estimated calibration equation significantly.
From regression analysis (see table 4) it follows that

the standard error of the estimated calibration factor c_α is σ_α=0.3%.
The resulting calibrated angle of attack α_c and the originally computed angle of attack α are both plotted in figure 7 at Mach number 0.72 and increasing normal loads: n=1.0,1.5,2.0.
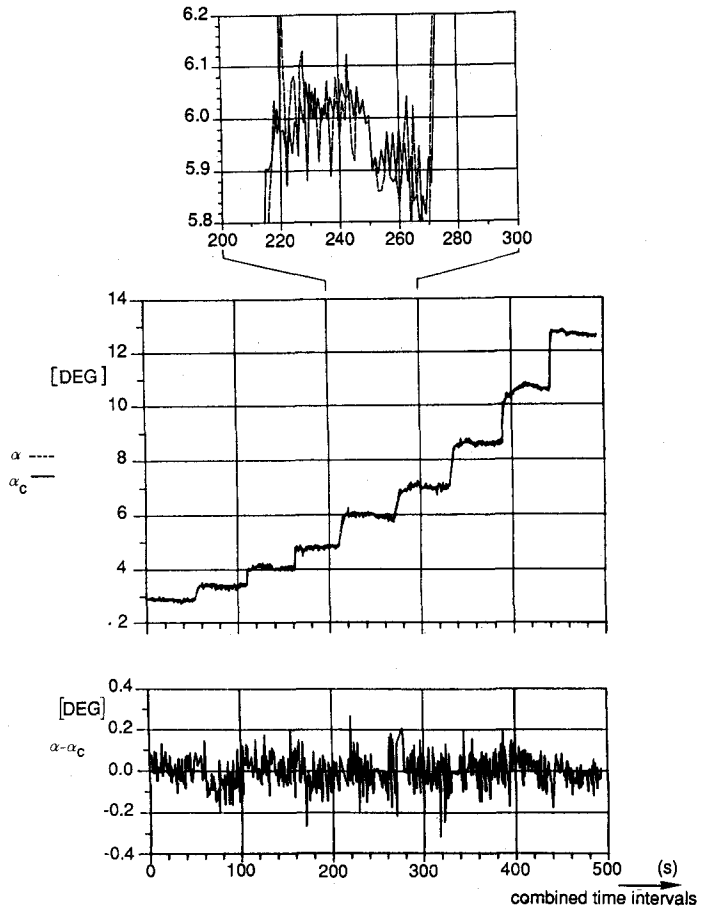

FIGURE 6 - The computed angle of attack α and the calibrated angle of attack α_c

TABLE 4   Calibration equation as result of regression analysis

Mach number range:

coefficient	M<0.4 value	standard error	0.7<M<0.8 value	standard error
c_o	0.0603	0.00067	0.0322	0.00096
c_α	0.5671	0.00097	0.6828	0.00158
c_M	0.0109	0.00199	0.0737	0.00138
c_{qV}	1.0000*	0.00000	1.0000*	0.00000
c_R	0.0000*	0.00000	0.0016	0.00003
c_{RB}	0.0000*	0.00000	0.0000*	0.00000

total correlation: 0.99994   0.98676

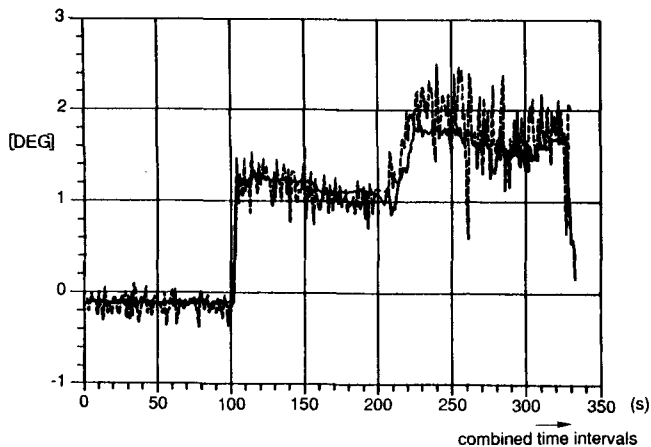The coefficients marked by * were fixed (not estimated).

1501

FIGURE 7 - The computed angle of attack $\alpha(- - -)$ and the calibrated angle of attack α_c (————) at M=0.72

5.3 Application of the calibration equation to the measured data

The calibrated angle of attack was computed using:

$$\alpha_c = c_o + \tfrac{1}{2}c_\alpha(\alpha_1+\alpha_2) + c_M M + 14c_{qv}q/V \qquad (19)$$

The angle of attack α computed from the pressure altitude variation together with the calibrated angle of attack α_c is shown in the figures 6 and 7.

For further analysis of the pressure distribution measurements the calibrated angle of attack α_c will be used instead of α because α is corrupted with much more noise than α_c. Note that α_c is the momentaneous angle of attack of the aircraft measured relative to the surrounding air, and is therefore the basic parameter on which the pressure distribution (airload) depends.

The final accuracies are listed in table 5.

TABLE 5   Estimated accuracies of the results

parameter	maximum unaccuracy	remarks
α_c	0.05 deg	due to the accuracy of the IRS
c_1	2%	observed spread in the final results (the pressure belts do not affect c_1 significantly since the effect at the lower side cancel out against the upper side during the integration)
$c_{1\alpha}$	2%	almost identical to the accuracy of c_1
M	0.001	as a result of p_i, p_s and PEC unaccuracies
$\Delta\theta$	0.1 deg	due to uncertainty in the stiffness data

table 5 continued

$\Delta c_{1\alpha}(Re_c)$	2%	remaining difference after corrections in $c_{1\alpha}$ between flight and windtunnel data

6. Comparison of flight data with windtunnel data

The flight test data were compared to HST (High Speed Tunnel at NLR) windtunnel test data taken using a 1:20 scale model (the measurement sections are shown in Fig. 1). Since in-flight test conditions and measurement sections are generally different from those in the windtunnel, interpolations of windtunnel data to flight conditions or vice versa had to be made.
The in-flight lift coefficients are derived by integration of the chordwise pressure distributions during each scanivalve cycle.

6.1 Comparison of local lift coefficients

Figure 8 presents a direct comparison between the midspan liftcurves as obtained from flight tests and windtunnel tests at transonic Mach numbers between M=0.742 and M=0.749. Because the Mach number varied during the flight tests, the two adjacent Mach numbers of the windtunnel test results are shown.
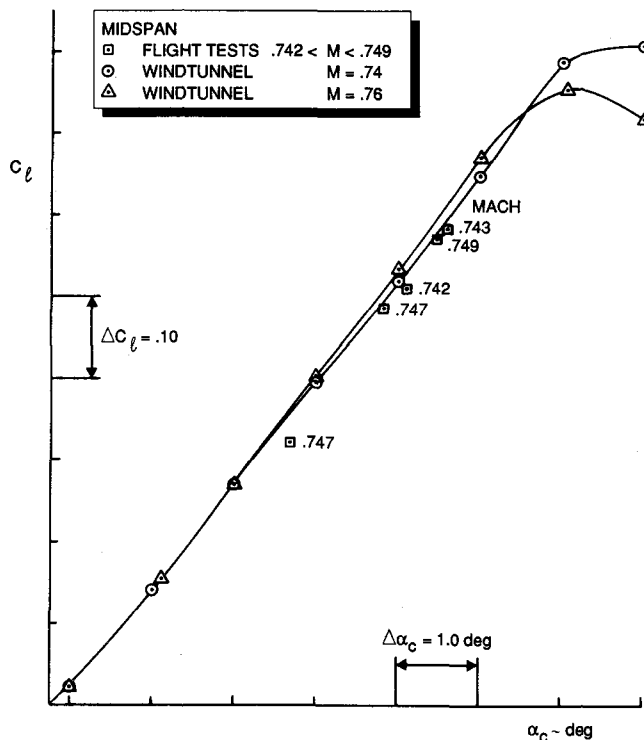

Figure 8 - Comparison of midspan lift curves
No corrections applied for differences in wing shape

A fair comparison can only be made when the difference in shape of the wing in the windtunnel with respect to the full-scale aircraft is taken into account for each condition.

The following factors concerning the differences
in wing shape were taken into account:
1. Deviation of the angle of attack along the span
   of the main wing due to production tolerances.
   Deviations of the contour of the airfoil
   sections due to production tolerances have been
   neglected; they are small in comparison to the
   dimensions of the pressure belt.
2. Deformation due to flight conditions (q_∞,Mach,
   α_c).

   2.a Windtunnel model deformation.
   2.b Aircraft deformation.
3. Deformation due to normal load condition (note:
   this deformation equals zero for the n=1g
   condition).
4. Deformation due to the presence of wing fuel.

Factors 2, 3 and 4 were determined using estimated
stiffness data. These stiffness data of the
aircraft were improved with results obtained from
ground vibration tests.

Lifting line theory was used to process these
differences in wing shape into a correction to the
spanwise lift distribution. The two-dimensional
section lift curve slope at a number of sections
(extracted from the spanwise lift distribution
based on windtunnel data) are input for the
required lifting line computations to determine
the correction on the spanwise lift distribution.

Figures 9 and 10 show comparisons of lift
coefficients versus the angle of attack for the
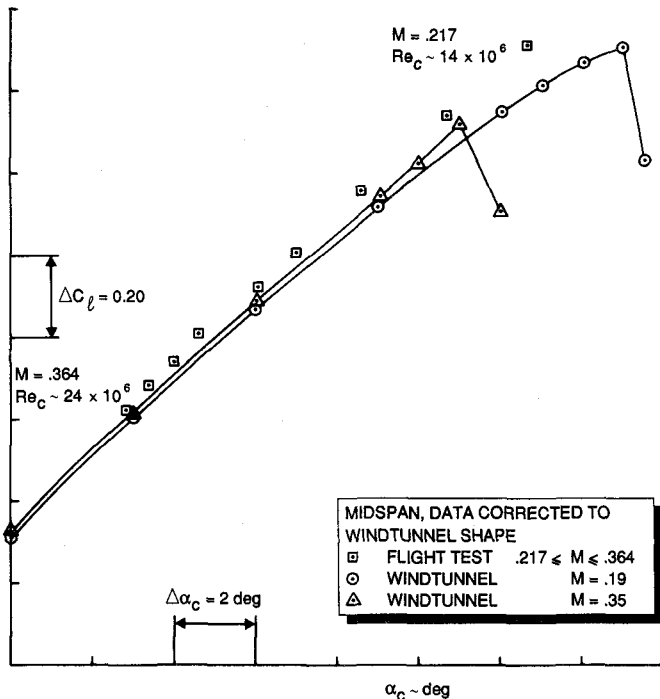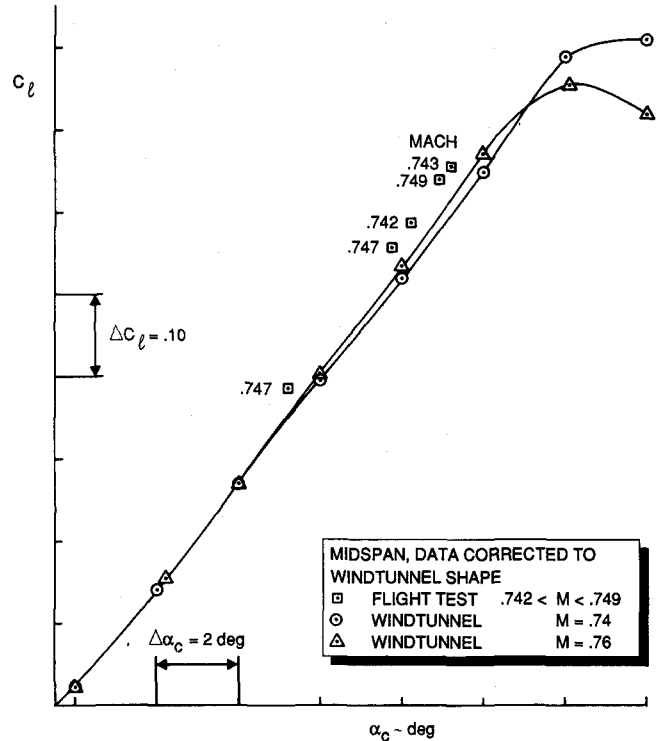midspan section at a low speed and at a transonic
condition.

Figure 10 - The lift coefficient at transonic
condition (midspan) as a function of the angle of
attack

The transition from laminar to turbulent boundary
layer was fixed at 5-7% chord in the windtunnel
tests. The Reynolds number (based on the mean
aerodynamic chord) varies from about 3 million in
the windtunnel to about 14 to 24 million for the
low speed flight conditions and to about 32
million for the transonic flight conditions.

Figure 11 shows lift curves obtained from flight
test data (corrected to windtunnel model shape as
well as uncorrected) and from windtunnel data at
three spanwise locations. The average Mach number
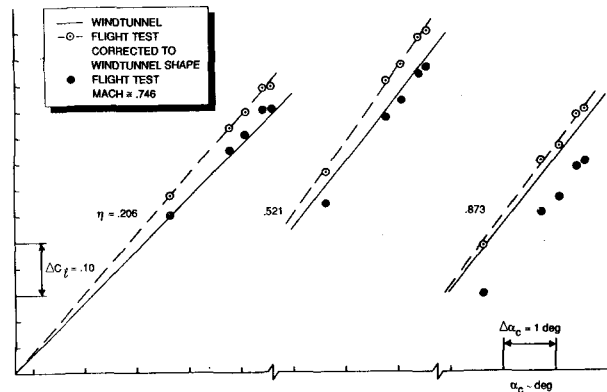during these flight tests was found to be M=.746.

Figure 9 - The lift coefficient at low speed condition
(midspan) as function of the angle of attack

Figure 11 - The lift coefficient at 3 wing stations as
a function of the angle of attack at Mach ≅.746

1503

The windtunnel data presented in this figure were obtained after linearization and interpolation between the eight available measurement sections and the two adjacent Mach numbers (M=.74 and M=.76). In figure 11 the observed change in slope of the section lift curves varies from about 13% at η=.206 to about 6% at η=.873.

Using the same change of Reynolds number (based on m.a.c.) from 3 to 32 million the DATCOM (Ref. 8) yields an increase of the slope of the section lift curves of about 6%. This value is valid for low Mach number conditions. Windtunnel tests (HST at NLR) on a Fokker 100 halfmodel reveal that the Reynolds number hardly affects the angle of attack for zero (tail-off) lift, α_{CLTO}=0. Furthermore, these windtunnel tests indicated an increase of the tail-off liftcurve slope of about 5% as a result of a change in Reynolds number from 3 to 8 million for the same Mach number. It is therefore considered that the observed differences in lift curve slope as shown in figure 11 between flight (corrected to windtunnel shape) and windtunnel are mainly caused by the Reynolds number effect.

6.2 Comparison of pressure distributions

Figure 12 shows a comparison of pressure distributions as obtained from windtunnel tests and flight tests for a transonic flight condition (no corrections were applied for differences in wing shape). The reduced aerodynamic loading in the tip region due to the deformation of the wing is most pronounced in the suction peak at the lower surface. For this case the local difference in wing angle of incidence between the windtunnel and flight tests is estimated to be $\Delta\Theta$=-0.9 deg at η=.873.
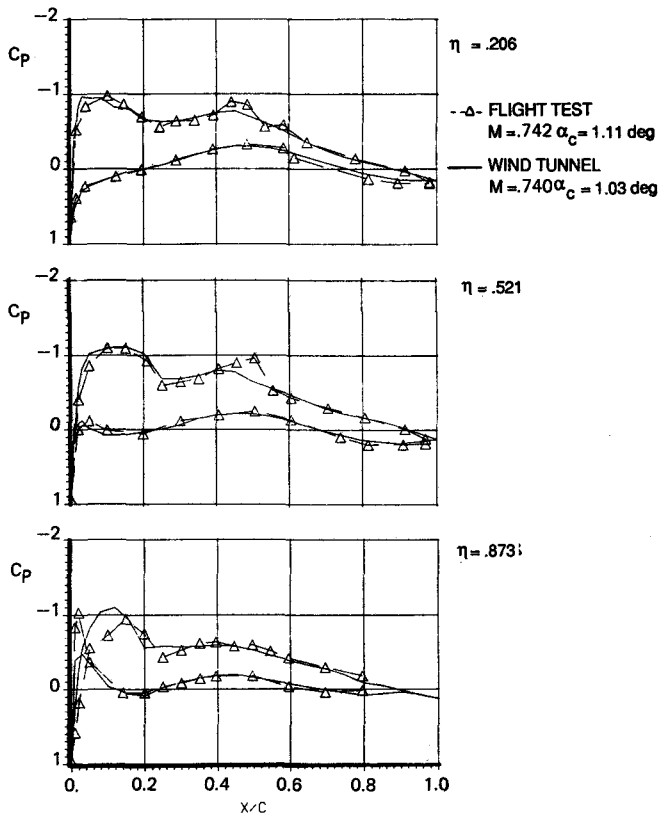
Figure 12 - Comparison of wing pressure distributions at three spanwise locations. No corrections applied for differences in wing shape. The (calibrated) angles of attack and the Mach numbers are approximately equal.

Figure 13 shows a comparison of flight test data with computed results of the computer program XFLO22 (Ref. 9). The XFLO22 computations were performed for the deformed wing while the midspan section lift was matched. Excellent agreement was obtained between the computed results and the flight test data.

Comparison of windtunnel data with flight test data show similar trends as shown in figure 12 (e.g. differences in the shock position, in the trailing-edge pressure and in the aftloading being typical Reynolds number effects). It is concluded that the observed differences in pressure distributions between flight and windtunnel data are mainly due to Reynolds number effects, since corrections for wing deformation have been taken into account.
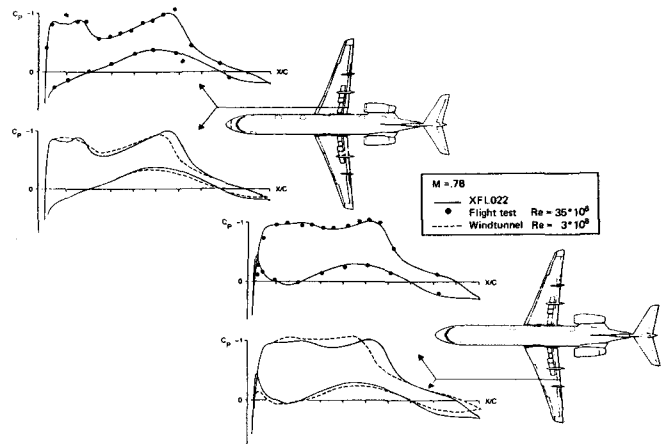
Figure 13 - Computed and measured wing pressures (wind tunnel and flight) The c_1 at midspan was matched, copied from Ref. 9

7. Conclusions

Accurate calibration of the flight angle of attack, which turned out to be dependent on the Mach number, is of major importance for validation and interpretation of in-flight pressure distribution measurement results. Regression analysis based on the pressure altitude variation enables the calibration of the angle of attack vanes to be determined with an accuracy of 0.05 deg. After correction for differences in wing shape reasonable agreement with windtunnel data was found. The remaining discrepancies between lift curve slopes can largely be attributed to the Reynolds number effect. For the prediction of accurate aerodynamic wing loads both Reynolds number effect and wing deformation must be accounted for. The accuracy of the local lift, derived from the in-flight measurement of the pressure distribution, is certainly better than 2% in all cases.

8. References

1 D.L.Loving Wind-tunnel-flight correlation
of shock-induced separated
flow.
NASA TN D-3580
Washington,D.C. sept. 1966.

2 G.C.Browne A comparison of Wing Pressure
T.E.B.Bateman Distributions Measured in
M.Pavitt Flight and on a Windtunnel
A.B. Haines Model of the Super VC.10.
R.&M. No. 3707 1972.

3 S.Weislogel GA(W)-2 Airfoil Flight Test
G.M.Gregorek Evaluation.
M.J.Hoffman SAE Paper 760492
Wichita, Kansas, april 1976.

4 L.C.Montoya F-8 Supercritical wing flight
R.D. Banner pressure, boundary-layer, and
wake measurements and
comparisons with windtunnel
data.
NASA TM X-3544
Washington,D.C. june 1977.

5 A.Bertelrud Correlation of global and local
aerodynamic properties in
flight.
Aviation and Astronautics 25th
annual conference.
Tel Aviv, Israel. febr. 1983.

6 Staff of Douglas DC-10 Winglet Flight
Aircraft Company Evaluation.
NASA CR-3704
june 1983.

7 S.L.Buckingham A flight test investigation
into flow separation and
structural response for a
transport aircraft at buffet
onset.
RAE TR 87006
Bedford, UK jan. 1987.

8 D.E.Hoak USAF STABILITY AND CONTROL
D.E.Ellison DATCOM
Ohio, august 1968.

9 N.Voogt CFD applications in design and
W.J.A.Mol analysis of the Fokker 50 and
J.Stout Fokker 100
D.F.Volkers AGARD CPD437
Lisbon 2-5 mei 1988.